Int. Conference on Boundary and Interior Layers
BAIL 2006
G. Lube, G. Rapin (Eds)

On the implementation of the $k-\varepsilon$ turbulence model in incompressible flow solvers based on a finite element discretization

D. Kuzmin and O. Mierka

Institute of Applied Mathematics (LS III), University of Dortmund
Vogelpothsweg 87, D-44227, Dortmund, Germany

kuzmin@math.uni-dortmund.de, omierka@math.uni-dortmund.de

1. Introduction

Turbulence plays an important role in many chemical engineering processes (fluid flow, mass and heat transfer, chemical reactions) which are dominated by convective transport. Since the direct numerical simulation (DNS) of turbulent flows is still prohibitively expensive, eddy viscosity models based on the Reynolds Averaged Navier-Stokes (RANS) equations are commonly employed in CFD codes. One of the most popular ones is the standard $k-\varepsilon$ model which has been in use since the 1970s. However, its practical implementation and, especially, the near-wall treatment has always been some somewhat of a mystery. Algorithmic details and employed 'tricks' are rarely reported in the literature, so that a novice to this area of CFD research often needs to reinvent the wheel. The numerical implementation of turbulence models involves many algorithmic components all of which may have a decisive influence on the quality of simulation results. In particular, a positivity-preserving discretization of the troublesome convective terms is an important prerequisite for the robustness of the numerical algorithm. This paper presents a detailed numerical study of the $k-\varepsilon$ model implemented in the open-source software package FeatFlow (`http://www.featflow.de`) using *algebraic flux correction* to enforce the positivity constraint [1, 2]. Emphasis is laid on a new implementation of wall functions, whereby the boundary conditions for k and ε are prescribed in a weak sense. Furthermore, the advantages of Chien's low-Reynolds number modification are explored. Two representative benchmark problems are used to evaluate the performance of the proposed algorithms in 3D.

2. Implementation of the $k-\varepsilon$ turbulence model

2..1. Mathematical model

In the framework of eddy viscosity models, the hydrodynamic behavior of a turbulent incompressible fluid is governed by the RANS equations for the velocity $\mathbf{u}$ and pressure p

$$\frac{\partial \mathbf{u}}{\partial t}+\mathbf{u}\cdot\nabla\mathbf{u}=-\nabla p+\nabla\cdot\left((\nu+\nu_T)[\nabla\mathbf{u}+\nabla\mathbf{u}^T]\right),\quad \nabla\cdot\mathbf{u}=0, \tag{1}$$

where ν depends only on the physical properties of the fluid, while ν_T is the turbulent eddy viscosity which is supposed to emulate the effect of unresolved velocity fluctuations $\mathbf{u}'$.

If the standard $k-\varepsilon$ model is employed, then $\nu_T=C_\mu\frac{k^2}{\varepsilon}$, where k is the turbulent kinetic energy and ε is the dissipation rate. Hence, the above PDE system is to be complemented by two additional convection-diffusion-reaction equations for computation of k and ε

$$\frac{\partial k}{\partial t}+\nabla\cdot\left(k\mathbf{u}-\frac{\nu_T}{\sigma_k}\nabla k\right)=P_k-\varepsilon, \tag{2}$$

$$\frac{\partial \varepsilon}{\partial t}+\nabla\cdot\left(\varepsilon\mathbf{u}-\frac{\nu_T}{\sigma_\varepsilon}\nabla\varepsilon\right)=\frac{\varepsilon}{k}(C_1P_k-C_2\varepsilon), \tag{3}$$

where $P_k = \frac{\nu_T}{2}|\nabla\mathbf{u} + \nabla\mathbf{u}^T|^2$ and ε are responsible for production and dissipation of turbulent kinetic energy, respectively. The default values of the involved empirical constants are as follows: $C_\mu = 0.09,\ C_1 = 1.44,\ C_2 = 1.92,\ \sigma_k = 1.0,\ \sigma_\varepsilon = 1.3$. Last but not least, equations (1)–(3) are to be endowed with appropriate initial/boundary conditions which will be discussed later.

2..2. Iterative solution strategy

The discretization in space is performed by an unstructured grid finite element method. The incompressible Navier-Stokes equations are discretized using the nonconforming $\tilde{Q}_1/Q_0$ element pair, whereas standard Q_1 elements are employed for k and ε. After an implicit time discretization by the Crank-Nicolson or backward Euler method, the nodal values of $(\mathbf{v}, p)$ and (k, ε) are updated in a segregated fashion within an outer iteration loop (see below).

For our purposes, it is worthwhile to introduce an auxiliary parameter $\gamma = \epsilon/k$, which makes it possible to decouple the transport equations (2)–(3) as follows [3]

$$\frac{\partial k}{\partial t} + \nabla\cdot\left(k\mathbf{u} - \frac{\nu_T}{\sigma_k}\nabla k\right) + \gamma k = P_k, \tag{4}$$

$$\frac{\partial \varepsilon}{\partial t} + \nabla\cdot\left(\varepsilon\mathbf{u} - \frac{\nu_T}{\sigma_\varepsilon}\nabla \varepsilon\right) + C_2\gamma\varepsilon = \gamma C_1 P_k. \tag{5}$$

This representation provides a positivity-preserving linearization of the sink terms, whereby the parameters ν_T and γ are evaluated using the solution from the previous outer iteration [2, 4].

The iterative solution process is based on the following hierarchy of nested loops

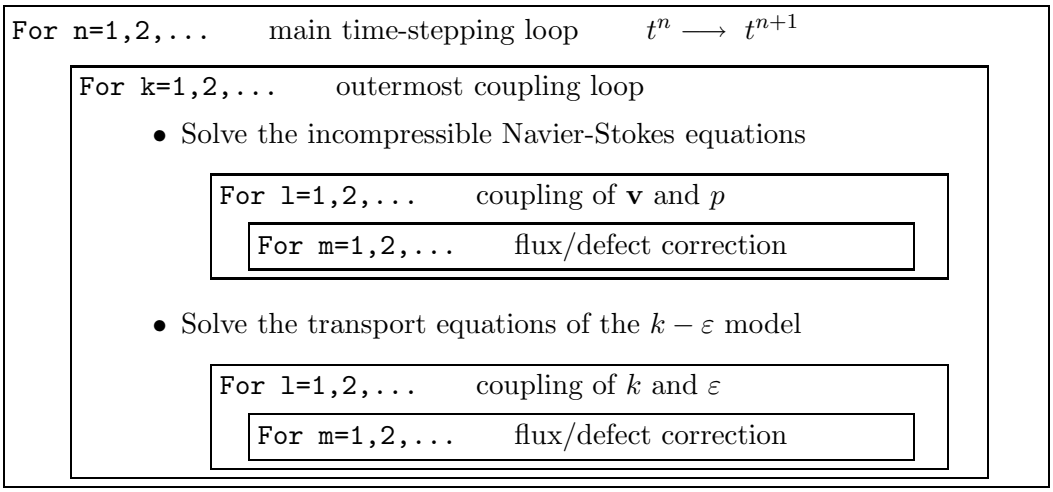

At each time step (one $n-loop$ iteration), the governing equations are solved repeatedly within the outer k-*loop* which contains the two subordinate l-*loops* responsible for the coupling of variables within the corresponding subproblem. The embedded m-*loops* correspond to iterative flux/defect correction for the involved convection-diffusion operators. Flux limiters of TVD type are activated in the vicinity of steep gradients, where nonlinear artificial diffusion is required to suppress nonphysical undershoots and overshoots. In the case of an implicit time discretization, subproblem (4)–(5) leads to a sequence of algebraic systems of the form [1, 2, 4]

$$A(\mathbf{u}^{(k)}, \gamma^{(l)}, \nu_T^{(k)})\Delta u^{(m+1)} = r^{(m)}, \qquad u^{(m+1)} = u^{(m)} + \omega\Delta u^{(m+1)}, \tag{6}$$

where $r^{(m)}$ is the defect vector and the superscripts refer to the loop in which the corresponding variable is updated. The predicted values $k^{(l+1)}$ and $\varepsilon^{(l+1)}$ are used to recompute the linearization parameter $\gamma^{(l+1)}$ for the next outer iteration (if any). The associated eddy viscosity ν_T is bounded from below by a certain fraction of the laminar viscosity $0 < \nu_{\min} \leq \nu$ and from above

by $\nu_{\max} = l_{\max}\sqrt{k}$, where $l_{\max}$ is the maximum admissible mixing length (the size of the largest eddies, e.g., the width of the domain). Specifically, we define the limited mixing length l_* as

$$l_* = \begin{cases} C_\mu \frac{k^{3/2}}{\varepsilon} & \text{if} \quad C_\mu k^{3/2} < \varepsilon l_{\max} \\ l_{\max} & \text{otherwise} \end{cases} \tag{7}$$

and calculate the turbulent eddy viscosity ν_T from the formula

$$\nu_T = \max\{\nu_{\min}, l_*\sqrt{k}\}. \tag{8}$$

The resulting value of ν_T is used to update the linearization parameter

$$\gamma = C_\mu \frac{k}{\nu_T}. \tag{9}$$

The above representation of ν_T and γ makes it possible to preclude division by zero and obtain bounded nonnegative coefficients without manipulating the actual values of k and ε.

2..2..1 Initial conditions

As a rule, it is rather difficult to devise a reasonable initial guess for a steady-state simulation or proper initial conditions for a dynamic one. If the velocity field is initialized by zero, it takes the flow some time to become fully turbulent. Therefore, we activate the $k-\varepsilon$ model at a certain time $t_* > 0$ after the startup. During the 'laminar' initial phase ($t \le t_*$), a constant effective viscosity $\nu_0 = \mathcal{O}(\nu)$ is prescribed. The values to be assigned to k and ε at $t = t_*$ are uniquely defined by the choice of ν_0 and of the default mixing length $l_0 \in [l_{\min}, l_{\max}]$ where the threshold parameter $l_{\min}$ corresponds to the size of the smallest admissible eddies. We have

$$k_0 = \left(\frac{\nu_0}{l_0}\right)^2, \qquad \varepsilon_0 = C_\mu \frac{k_0^{3/2}}{l_0} \qquad \text{at} \quad t \le t_*. \tag{10}$$

Alternatively, the initial values of k and ε can be estimated by means of a zero-equation (mixing length) turbulence model or computed using an extension of the inflow or wall boundary conditions (see below) into the interior of the computational domain.

2..2..2 Boundary conditions

At the inflow boundary Γ_{in} we prescribe all velocity components and the values of k and ε:

$$\mathbf{u} = \mathbf{g}, \qquad k = c_{bc}|\mathbf{u}|^2, \qquad \varepsilon = C_\mu \frac{k^{3/2}}{l_0} \qquad \text{on} \quad \Gamma_{\text{in}}, \tag{11}$$

where $c_{bc} \in [0.003, 0.01]$ is an empirical constant and $|\mathbf{u}| = \sqrt{\mathbf{u}\cdot\mathbf{u}}$ is the Euclidean norm of the velocity. At the outlet Γ_{out}, the normal gradients of all variables are set equal to zero, which corresponds to the Neumann ('do-nothing') boundary condition:

$$\mathbf{n}\cdot[\nabla\mathbf{u} + \nabla\mathbf{u}^T] = \mathbf{0}, \qquad \mathbf{n}\cdot\nabla k = 0, \qquad \mathbf{n}\cdot\nabla\varepsilon = 0 \qquad \text{on} \quad \Gamma_{\text{out}}. \tag{12}$$

In the finite element framework, these homogeneous boundary conditions imply that the surface integrals resulting from integration by parts in the variational formulation vanish.

At an impervious solid wall Γ_w, the normal component of the velocity is set equal to zero

$$\mathbf{n}\cdot\mathbf{u} = 0 \qquad \text{on} \quad \Gamma_w \tag{13}$$

whereas tangential slip is permitted in turbulent flow simulations. The practical implementation of the above no-penetration ('free slip') boundary condition is nontrivial if the boundary of the

computational domain is not aligned with the axes of the Cartesian coordinate system. In this case, condition (13) is imposed on a linear combination of several velocity components whereas their boundary values are unknown. Therefore, standard implementation techniques based on a modification of the corresponding matrix rows cannot be used.

In order to set the normal velocity component equal to zero, we nullify the off-diagonal entries of the preconditioner $A(\mathbf{u}^{(m)}) = \{a_{ij}^{(m)}\}$ in the defect correction loop for the momentum equation [2, 4]. This enables us to compute the boundary values of the vector $\mathbf{u}$ explicitly before solving a sequence of linear systems for the velocity components:

$$a_{ij}^{(m)} := 0, \quad \forall j \neq i, \qquad \mathbf{u}_i^* := \mathbf{u}_i^{(m)} + \mathbf{r}_i^{(m)}/a_{ii}^{(m)} \qquad \text{for} \quad \mathbf{x}_i \in \Gamma_w. \tag{14}$$

In the next step, we project the predicted values $\mathbf{u}_i^*$ onto the tangent vector/plane and constrain the corresponding entry of the defect vector $\mathbf{r}_i^{(m)}$ to be zero

$$\mathbf{u}_i^{(m)} := \mathbf{u}_i^* - (\mathbf{n}_i \cdot \mathbf{u}_i^*)\mathbf{n}_i, \qquad \mathbf{r}_i^{(m)} := 0 \qquad \text{for} \quad \mathbf{x}_i \in \Gamma_w. \tag{15}$$

After this manipulation, the corrected values $\mathbf{u}_i^{(m)}$ act as Dirichlet boundary conditions for the solution $\mathbf{u}_i^{(m+1)}$ at the end of the defect correction step. As an alternative to the implementation technique of predictor-corrector type, the projection can be applied to the residual vector rather than to the nodal values of the velocity:

$$a_{ij}^{(m)} := 0, \quad \forall j \neq i, \qquad \mathbf{r}_i^{(m)} := \mathbf{r}_i^{(m)} - (\mathbf{n}_i \cdot \mathbf{r}_i^{(m)})\mathbf{n}_i \qquad \text{for} \quad \mathbf{x}_i \in \Gamma_w. \tag{16}$$

For Cartesian geometries, the modifications to be performed affect just one velocity component (in the normal direction) as in the case of standard Dirichlet boundary conditions.

2..2..3 Wall functions

To complete the problem statement, we still need to prescribe the tangential stress as well as the boundary conditions for k and ε on Γ_w. Note that the equations of the $k-\varepsilon$ model are invalid in the vicinity of the wall where the Reynolds number is rather low and viscous effects are dominant. In order to avoid the need for resolution of strong velocity gradients, *wall functions* are typically applied at an internal boundary Γ_y located at a distance y from the solid wall Γ_w

$$\mathbf{n} \cdot [\nabla \mathbf{u} + \nabla \mathbf{u}^T] = -\frac{u_\tau^2}{\nu_T} \frac{\mathbf{u}}{|\mathbf{u}|}, \qquad k = \frac{u_\tau^2}{\sqrt{C_\mu}}, \qquad \varepsilon = \frac{u_\tau^3}{\kappa y} \qquad \text{on} \quad \Gamma_y, \tag{17}$$

where $\kappa = 0.41$ is the von Kármán constant. The above mentioned free-slip condition (13) is also to be imposed on Γ_y rather than on Γ_w. Therefore, $\mathbf{u}$ is the tangential velocity which can be used to compute the friction velocity u_τ from the nonlinear equation

$$\frac{|\mathbf{u}|}{u_\tau} = \frac{1}{\kappa} \log y^+ + \beta \tag{18}$$

valid in the *logarithmic layer*, where the local Reynolds number $y^+ = \frac{u_\tau y}{\nu}$ is in the range $11.06 \leq y^+ \leq 300$. The empirical constant β equals 5.2 for smooth walls.

Strictly speaking, a boundary layer of width y should be removed from the computational domain Ω. However, it is supposed to be very thin, so that the equations can be solved in the whole domain Ω with wall functions prescribed on the boundary part Γ_w rather than on Γ_y. Since the choice of y is rather arbitrary, it is worthwhile to define the boundary layer width by fixing y_+, as proposed in [3, 5]. The implicitly defined $y = \frac{\nu y_+}{u_\tau}$ is assumed to be the point where the logarithmic layer meets the viscous sublayer so that y_+ satisfies (18) as well as the linear relation $y_+ = \frac{|\mathbf{u}|}{u_\tau}$. The corresponding parameter value y_+^* is given by

$$y_+^* = \frac{1}{\kappa} \log y_+^* + \beta \approx 11.06 \qquad \text{on} \quad \Gamma_y. \tag{19}$$

The use of y_+^* in the wall laws (17)-(19) yields an explicit relation for the friction velocity u_τ which is required to evaluate the tangential stress for the momentum equations [5]

$$\mathbf{n}\cdot[\nabla\mathbf{u}+\nabla\mathbf{u}^T]=-\frac{u_\tau^*}{\nu_T}\frac{\mathbf{u}}{y_+^*},\qquad \text{where}\quad u_\tau^*=\max\left\{C_\mu^{0.25}\sqrt{k},\frac{|\mathbf{u}|}{y_+^*}\right\}. \tag{20}$$

This expression provides a natural boundary condition for the tangential velocity

$$\int_{\Gamma_w}\nu_T(\mathbf{n}\cdot[\nabla\mathbf{u}+\nabla\mathbf{u}^T]\cdot\mathbf{w})\,ds=-\int_{\Gamma_w}\frac{u_\tau^*}{y_+^*}\,(\mathbf{u}\cdot\mathbf{w})\,ds. \tag{21}$$

Due to (17), the boundary value of the turbulent eddy viscosity is proportional to ν

$$\nu_T=c_\mu\frac{k^2}{\varepsilon}=\kappa u_\tau y=\kappa y_*^+\nu. \tag{22}$$

Of course, the above relation is satisfied automatically if the boundary conditions for k and ε are implemented in the strong sense as proposed in [2, 4]. However, the use of Dirichlet boundary conditions means that the boundary values of k and ε depend solely on the friction velocity $u_\tau=\frac{|\mathbf{u}|}{y_+^*}$ which is proportional to the flow velocity at the wall. This results in a one-way coupling of the boundary conditions which is rather unrealistic. In order to let k and ε 'float' and influence the momentum equations via (20)-(21), the wall boundary conditions should be implemented in a weak sense. To this end, let us compute the boundary values of ν_T from equation (22) and invoke (17) to retrieve the normal derivatives of k and ε as follows [5]

$$\mathbf{n}\cdot\nabla k=-\frac{\partial k}{\partial y}=0,\qquad \mathbf{n}\cdot\nabla\varepsilon=-\frac{\partial\varepsilon}{\partial y}=\frac{u_\tau^3}{\kappa y^2}=\frac{1}{\nu_T}\frac{u_\tau^5}{y_+\nu}. \tag{23}$$

These natural boundary conditions are to be plugged into the surface integrals resulting from integration by parts in the variational formulation for equations (4) and (5)

$$\int_{\Gamma_w}\frac{\nu_T}{\sigma_k}(\mathbf{n}\cdot\nabla k)w\,ds=0,\qquad \int_{\Gamma_w}\frac{\nu_T}{\sigma_\varepsilon}(\mathbf{n}\cdot\nabla\varepsilon)w\,ds=\int_{\Gamma_w}\frac{1}{\sigma_\varepsilon}\frac{u_\tau^5}{y_+\nu}w\,ds. \tag{24}$$

Furthermore, it is commonly assumed that $P_k=\varepsilon$ in the wall region, so that the correct boundary value of the production term must be computed from

$$P_k=\frac{u_\tau^3}{\kappa y}=\frac{u_\tau^3}{\nu_T}\frac{|\mathbf{u}|}{y_+^*},\qquad \text{where}\quad u_\tau=C_\mu^{0.25}\sqrt{k}. \tag{25}$$

The above implementation of wall functions is largely based on the publication of Grotjans and Menter [5] which should be consulted for further algorithmic details.

2..2..4 Chien's Low-Reynolds $k-\varepsilon$ modification

In the previous section, the implementation of the standard $k-\varepsilon$ model was considered, whereby wall functions were prescribed on Γ_w in order to eliminate the need for a costly integration to the wall. However, the validity of wall functions is limited to flat-plate boundary layers and developed flow conditions, whereas for accurate simulations of complex flows the model should be extended with appropriate Low-Reynolds modifications. Another reason for their implementation is that for turbulent flows characterized by rather low Reynolds numbers the removed region could occupy a significant part of the domain and, therefore, play an important role. One of the most commonly used Low-Reynolds modifications is that proposed by Chien [6]. It features nice numerical properties and comes with remarkably simple boundary conditions

$$\mathbf{u}=0,\quad k=0,\quad \tilde{\varepsilon}=0\quad\text{on}\quad\Gamma_w, \tag{26}$$

where the dissipation rate is redefined as $\varepsilon = \tilde{\varepsilon} + 2\nu k/y^2$. Furthermore, the following damping functions are introduced to provide a smooth transition from the laminar to the turbulent regime

$$f_\mu = 1 - \exp(-0.0115y^+), \qquad f_2 = 1 - 0.22\exp\left(\frac{k^2}{6\nu\tilde{\varepsilon}}\right)^2. \tag{27}$$

The resulting generalization of equations (4)–(5) to the case of low Reynolds numbers reads

$$\frac{\partial k}{\partial t} + \nabla\cdot\left(k\mathbf{u} - \frac{\nu_T}{\sigma_k}\nabla k\right) + \left(\gamma + \frac{2\nu}{y^2}\right)k = P_k, \qquad \nu_T = C_\mu f_\mu k^2/\tilde{\varepsilon}, \tag{28}$$

$$\frac{\partial \tilde{\varepsilon}}{\partial t} + \nabla\cdot\left(\tilde{\varepsilon}\mathbf{u} - \frac{\nu_T}{\sigma_\varepsilon}\nabla\tilde{\varepsilon}\right) + \left(C_2 f_2\gamma + \frac{2\nu}{y^2}\exp(-0.5y^+)\right)\tilde{\varepsilon} = \gamma C_1 P_k. \tag{29}$$

The new definition of the turbulent eddy viscosity is in accordance with the DNS results which reveal that the ratio $f_\mu = \frac{\nu_T\tilde{\varepsilon}}{C_\mu k^2}$ is not a constant but a function approaching zero at the wall.

Note that the extra sink terms in (28) and (29) have positive coefficients and pose no hazard to positivity of the numerical solution. As before, the linearization parameter γ is recomputed in every outer iteration of the $l-$loop. The local Reynolds number y^+ depending on the friction velocity $u_\tau(\mathbf{u}^{(k)})$ is updated at the beginning of the $k-$loop as follows: $u_\tau = \sqrt{\nu\frac{\partial v_t}{\partial n}}$, where n is the unit normal to the wall and v_t is the tangential velocity at the nearest wall point. Moreover, the update of y^+ requires knowing the distance to the wall. In the current implementation, it is computed in a brute-force way as the distance to the nearest midpoint of a boundary edge/face projected onto the uniquely defined normal associated with this edge/face. Alternatively, the computation of the distance can be performed using one of the numerous redistancing/reinitialization algorithms developed in the framework of level set methods.

3. Numerical examples

3..1. Channel flow

The validation of the implemented Chien's Low-Reynolds $k-\varepsilon$ model was performed on the basis of the channel flow benchmark problem. The reference data were provided by Kim's DNS simulation [7] for $\mathrm{Re}_\tau = 395$ which is based on the friction velocity u_τ, half of the channel width d and kinematic viscosilty ν. In order to obtain the developed flow conditions required for validation, the inlet/outlet boundary conditions on the reduced domain were interchanged several times during the computation. The almost mesh-independent solution was obtained on the 4th multigrid level using $50,000$ elements and local mesh refinement in the near-wall region.

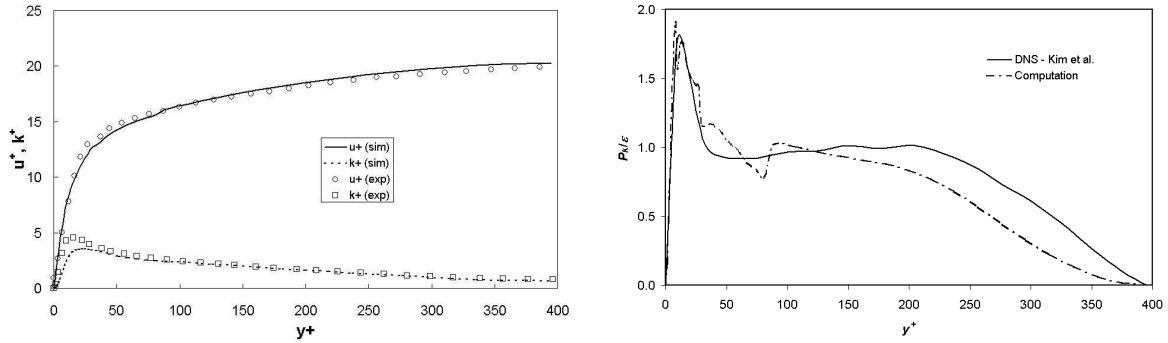

Figure 1: Nondimensional velocity profiles of the streamline velocity component u^+, turbulent kinetic energy k^+ (left) and the ratio of production/dissipation rates P_k/ε (right) for channel flow, $\mathrm{Re}_\tau = 395$. Reference DNS solutions by Kim *et al.* [7].

The distance from the wall boundary to the nearest interior point corresponds to $y^+ \approx 2$. The resulting profiles of the monitored nondimensional quantities (horizontal velocity component v_x, turbulent kinetic energy k as well as the ratio of its production and dissipation rates P_k/ε) displayed in Fig. 1 are in a good agreement with the reference data from [7].

3..2. Backward facing step

The second example deals with a 3D simulation of turbulent incompressible flow past a backward facing step using the $k-\varepsilon$ model with three different wall boundary treatments (wall functions implemented using Dirichlet and Neumann boundary conditions vs. the Low-Reynolds number modification based on (26)-(29)). The problem is solved for the Reynolds number $\mathrm{Re} = 47,625$ [8] as defined by the step height H, mean inflow velocity u_{mean} and kinematic viscoity ν. All simulations were performed on the same computational mesh consisting of approximately $260,000$ elements, see Fig. 2 (top). Local mesh refinement was employed in the vicinity of the walls and behind the step. The numerical solutions presented in Fig. 2 are in a good agreement with those published in the literature [8]. However, the influence of wall boundary conditions implemented in the strong or weak sense or by means of the Low-Reynolds modification is rather significant. The recirculation length $L_R = x_r/H$ predicted by the Low-Reynolds number version and wall functions with Neumann boundary conditions (24) is underestimated ($L_R \approx 5.4$), which is also the case for the computational results published in the literature ($5.0 < L_R < 6.5$, see [5, 8, 9]). On the other hand, the implementation of wall functions in the strong sense yields $L_R \approx 7.1$ which matches the experimentally measured recirculation length $L_R \approx 7.1$, see [10]. Unfortunately, this perfect agreement turns out to be a pure coincidence. The numerical solutions obtained using different kinds of boundary treatment are compared to one another and to experimental data [10] in Fig. 3, where 6 different crossplane velocity distributions $u_x/(u_x)_{\max}$ are plotted at different distances from the step. These profiles indicate that the use of natural boundary conditions (24) yields essentially the same results as the Low-Reynolds number version. In either case, the numerical solutions agree well with those presented in [5, 8, 9].

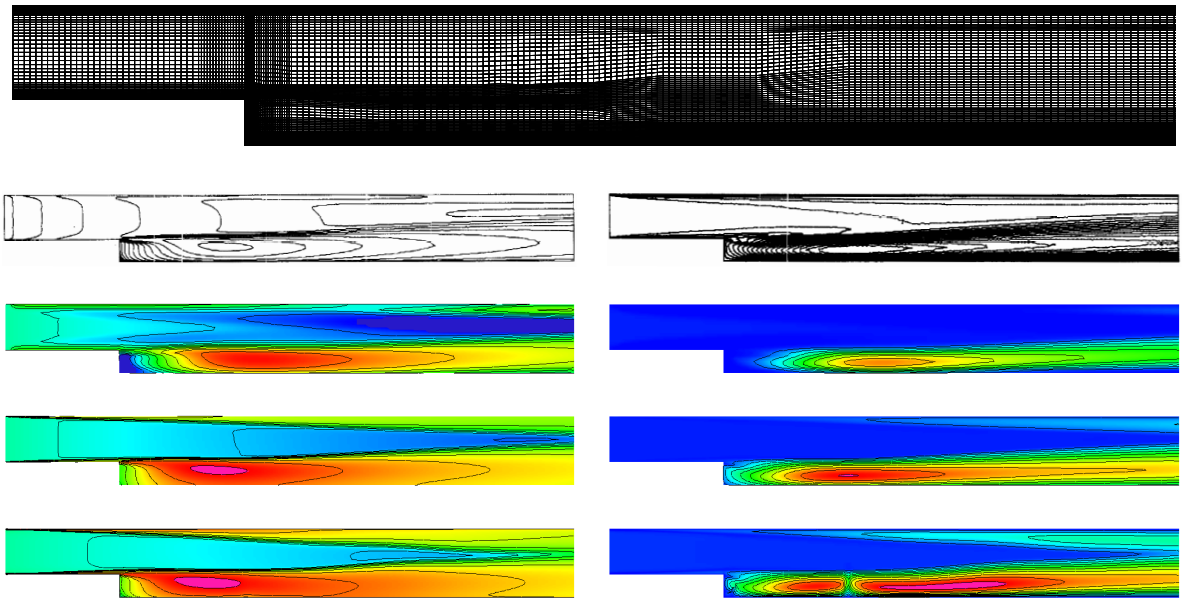

Figure 2: Computational mesh for the backward facing step problem (top) and steady-state profiles of the turbulent kinetic energy - $\ln k$ (left) and turbulent eddy viscosity - ν_T (right). From top to bottom: reference solution [7] vs. boundary treatment based on wall functions with Dirichlet BC, wall functions with Neumann BC, and Chien's Low-Reynolds number model.

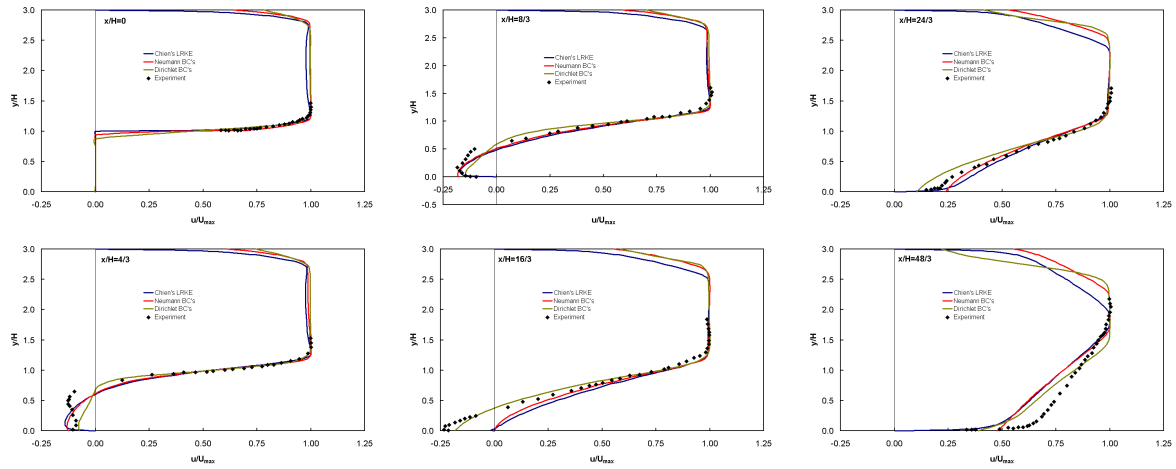

Figure 3: Velocity profiles u_x for 6 different distances x/H from the step computed using three different kinds of near-wall treatment for the $k-\varepsilon$ model.

References

[1] D. Kuzmin and M. Möller, Algebraic Flux Correction I. Scalar Conservation Laws. In: D. Kuzmin, R. Löhner and S. Turek (eds.) *Flux-Corrected Transport: Principles, Algorithms, and Applications*. Springer, 2005, 155-206.

[2] S. Turek and D. Kuzmin, Algebraic Flux Correction III. Incompressible Flow Problems. In: D. Kuzmin, R. Löhner and S. Turek (eds.) *Flux-Corrected Transport: Principles, Algorithms, and Applications*. Springer, 2005, 251-296.

[3] A. J. Lew, G. C. Buscaglia and P. M. Carrica, A Note on the Numerical Treatment of the k-epsilon Turbulence Model. *Int. J. of Comp. Fluid Dyn.* **14** (2001) 201–209.

[4] D. Kuzmin and S. Turek, Multidimensional FEM-TVD Paradigm for Convection-Dominated Flows. In: *Proceedings of the IV European Congress on Computational Methods in Applied Sciences and Engineering (ECCOMAS 2004)*, Volume II, ISBN 951-39-1869-6.

[5] H. Grotjans and F. Menter, Wall Functions for General Application CFD Codes. ECCOMAS 98, Proceedings of the 4th European Computational Fluid Dynamics Conference, John Wiley & Sons, 1998, pp. 1112-1117.

[6] K.-Y. Chien, Predictions of Channel and Boundary-Layer Flows with a Low-Reynolds-Number Turbulence Model. *AIAA J.* **20** (1982) 33–38.

[7] J. Kim, P. Moin and R. D. Moser, Turbulence Statistics in Fully Developed Channel Flow at Low Reynolds Number. *J. Fluid Mech.* **177** (1987) 133–166.

[8] F. Ilinca, J.-F. Hétu and D. Pelletier, A Unified Finite Element Algorithm for Two-Equation Models of Turbulence. *Comp. & Fluids* **27**-3 (1998) 291–310.

[9] S. Thangam, C. G. Speziale, Turbulent Flow Past a Backward-Facing Step: A Critical Evaluation of Two-Equation Models, *AIAA J.* **30**-5 (1992), 1314–1320.

[10] J. Kim, Investigation of Separation and Reattachment of Turbulent Shear Layer: Flow over a Backward Facing Step. *PhD Thesis*, Stanford University, 1978.